Journal of Materials Chemistry A

Accepted Manuscript

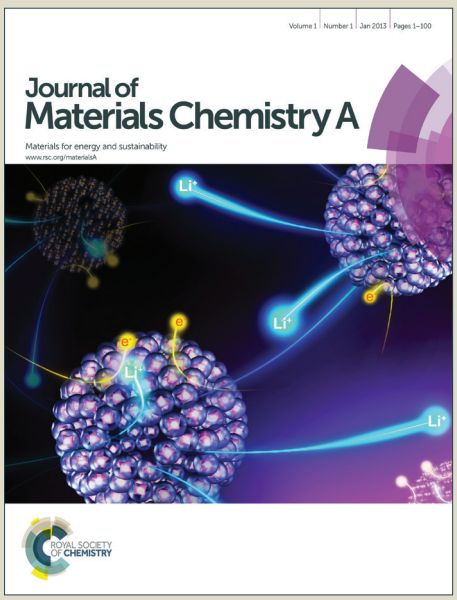

ROYAL SOCIETY OF CHEMISTRY

www.rsc.org/materialsA

Journal Name

RSCPublishing

ARTICLE

Construction of mass-controllable mesoporous $NiCo_2S_4$ electrodes for high performance supercapacitors

Cite this: DOI: 10.1039/x0xx00000x

Tao Peng,[a] Zhongyu Qian,[a] Jun Wang,*[a] Dalei Song,[a] Jinyuan Liu,[a] Qi Liu[a] and Peng Wang[b]

Received 00th January 2012,
Accepted 00th January 2012

DOI: 10.1039/x0xx00000x

www.rsc.org/

3D interconnected $NiCo_2S_4$ nanosheets have been directly grown on nickel foams through a facile two-step solution-based method. The as-prepared electrodes with controllable mass loadings and microstructures show excellent electrochemical performance, indicating their potential application for supercapacitors. Electrochemical measurements exhibit that the $NiCo_2S_4$/nickel foam electrode has a competitive areal specific capacitance (10.82 Fcm^{-2} at 10 $mAcm^{-2}$), relatively high rate capability (40.3% capacitance retention at 80 $mAcm^{-2}$) and good cycling stability (92% capacitance retention after 1500 cycles at 20 $mAcm^{-2}$).

1. Introduction

Pseudocapacitive materials have the potential of bridging supercapacitors (high power density) and batteries (high energy density) with reversible redox reactions occurring at or near the surface of an electrode.[1-3] Recent years, conductive matrix with nanostructures have achieved success with respect to robust interfaces and excellent performances.[4-6] However, most attentions have focused on the surface of conductive scaffolds with an integrated architecture, which may result in a high performance of the pseudocapacitive materials rather than of the electrodes.[7-9] To address all kinds of technological challenges, efforts needs to be paid to the entire electrode system and pore volume provided within the scaffolds from the surface.[10-12] Moreover, cost-effective and facile methods are still needed for scale-up.

Some simple strategies, such as slurry casting, could achieve the goal at cost of bulk agglomeration and extra weight of additives, but the lack in spatial precision may eradicate the advantages of nanoscale materials.[13-16] Moreover, intrinsic conductivity and contact resistance of these oxide materials still seriously limit their performance. While mesoporous nanostructures of electroactive materials grown directly on conductive substrates with a small mass loading needs to shift more towards systems engineering.[17-19] A key challenge for the fabrication is to build up an optimal physical space stepwisely with a large mass loading and guarantees a fast ion and electron transfer.

Spinel nickel cobaltite ($NiCo_2O_4$) has recently drawn much attention for pseudocapacitors because of their low cost, flexibility in morphology and high electrochemical activity.[18] However, its conductivity is too low to favor fast electron transport which may lead to low rate capability. To address this problem, efforts have been focused on the conversion of $NiCo_2O_4$ to $NiCo_2S_4$ which exhibited much higher electric conductivity than that of $NiCo_2O_4$.[16,21] For example, Xiao and co-workers obtained an areal capacitance of 2.86 Fcm^{-2} at 4 $mAcm^{-2}$ for a $NiCo_2S_4$ nanotube array electrode.[16] Jiang and co-workers developed a hydrothermal method to synthesize urchin-like $NiCo_2S_4$ nanostructures and obtained a high specific capacitance of 1149 Fg^{-1} at 1 Ag^{-1}.[21] But the binder they used in the fabrication of electrodes may eradicate the advantages of $NiCo_2S_4$. In addition, hydrothermal method needs higher temperature than solution-based method which results in more heat and more power dissipation.

As a proof-of-concept, we present a two-step solution-based method to produce electrodes with controllable mass loadings and microstructures (Sch.1). High mass loadings could be achieved with increased depositing numbers. Second, considering that high mass loadings always mean the poor ion and electron transports, and $NiCo_2S_4$ which shows much higher conductivity than $NiCo_2O_4$.[15-16,20-21] Therefore, shape-preserved $NiCo_2S_4$ could be obtained from $NiCo_2O_4$ via a facile anion exchange reaction (AER). As a result, the unique electrode shows a high areal capacitance (10.82 Fcm^{-2} at 10 $mAcm^{-2}$), outstanding rate capacitance (40.3% capacitance retention at 80

mAcm^{-2}) and excellent cycling stability (92% capacitance retention after 1500 cycles at 20 mAcm^{-2}), which make it a promising electrode for supercapacitors.

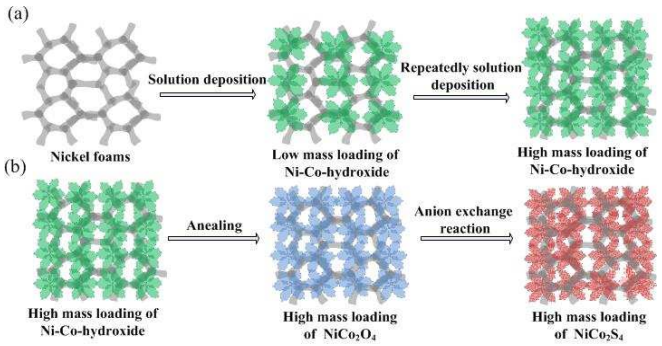

Sch.1 (a) Schematic image of control of mass loading on nickel foams; (b) Schematic image of the conversion of $NiCo_2O_4$ to $NiCo_2S_4$ via AER

2. Experimental

2.1 Preparation of $NiCo_2O_4$/nickel foam

All the chemicals were directly used after purchase without further purification. Solution deposition (SD) was performed by a method which was reported in the literature with minor modifications.[18] Nickel foams (50×25×1 mm^3, pores per inch: 110) were rolled to a thickness of 0.5 mm before use. The rolled nickel foams were immersed in a 3 M HCl solution for 15 min, then soaked in a 0.02 M $NiCl_2$ solution to prevent oxidation. 1.2 mmol of $Ni(NO_3)_2 \cdot 6H_2O$ and 2.4 mmol of $Co(NO_3)_2 \cdot 6H_2O$ were dispersed into a mixed solution of 48 mL deionized water and 24 ml ethanol , followed by the addition of 7.2 mmol of hexamethylenetetramine. The above nickel foam was dipped into a sealed bottle which contains the as-prepared solution, and the bottle was heated at 90 ℃ in a water bath for 5 h. The nickel foam after solution deposition was removed and washed with deionized water and absolute ethanol, then dried at 90 ℃. After that, the substrate with loaded Ni-Co-hydroxide was repeatedly dipped into a sealed bottle which contains the as-prepared solution and reacted on the above conditions. The deposition number are 1, 2, 3, 4, and the corresponding $NiCo_2S_4$/nickel foam samples were marked as D1, D2, D3, D4, respectively. The $NiCo_2O_4$ precursor was obtained by annealing the Ni-Co-hydroxide at 320℃ for 2 h with a heating rate of 2℃ min^{-1}.

2.2 Preparation of $NiCo_2S_4$/nickel foam

$NiCo_2S_4$ nanosheets were converted from $NiCo_2O_4$ nanosheets above. The as-prepared $NiCo_2O_4$ /nickel foam was dipped into a beaker which contains 0.05 M (80 mL) of Na_2S solution, and the beaker was heated at 90 ℃ in a water bath for 9 h. After AER, the nickel foam with loaded products was removed and washed with deionized water and absolute ethanol, then dried at 90 ℃.

2.3 Characterization

The morphology of the samples was investigated by scanning electron microscopy-energy dispersive spectroscopy (SEM-EDS) (JEOL JSM-6480A) and transmission electron microscopy (TEM) (Philips CM 200 FEG, 200 kV). The crystal phase of the materials were determined by means of X-ray diffraction (XRD) (Rigaku TTR-III, Cu K_α, λ = 0.15406 nm).The N_2 sorption measurement were conducted using TriStar II 3020 2.00 instrument at 195.850 °C (77 K). The near-surface elemental composition of the $NiCo_2S_4$ product was measured by X-ray photoelectron spectroscopy (XPS) (PHI 5700 ESCA System) and EDS (JEOL JSM-6480A).

2.4 Electrochemical Measurements

The electrochemical measurements were conducted using a CHI 760B electrochemistry workstation. A three-electrode system was used in the measurements which consisted of a working electrode, a platinum foil counter electrode (1×1 cm^2), a saturated calomel electrode (SCE) reference electrode, and electrolyte (6 M KOH aqueous solution). The as-prepared $NiCo_2S_4$ electrodes were served as working electrode with nominal area of 1×1 cm^2 and the mass loadings of the $NiCo_2S_4$ mesoporous nanosheets on nickel foam were 2.168, 4.464, 6.896, 9.984 mgcm^{-2} for D1, D2, D3, D4, respectively. The corresponding $NiCo_2O_4$/nickel foam electrode with mass loading of 2.181 mgcm^{-2} (noted as C1) also measured on above condition to compare with D1.

2.5 Calculations

For galvanostatic charge-discharge curves, C_m (F g^{-1}), C_s (F cm^{-2}), ESR (Ω), η (%) can be calculated according the following equations(1)-(4):

$$C_s = It/(A \Delta V) \quad (1)$$

$$C_m = It/(m \Delta V) \quad (2)$$

$$R = V_{drop}/(2I) \quad (3)$$

$$\eta = t_c/t \times 100\% \quad (4)$$

where I (A) is the discharge current, t is the discharge time (s), ΔV is the applied potential region (V), A refers to the area (cm^2) of the electrode, m (g) is the mass of the active materials, and V_{drop} (V) is estimated from the voltage drop at the beginning of the discharge curve, η (%) is columbic efficiency, t_c is the charge time (s).

3. Results and discussion

3.1 Control of mass loading on nickel foam via repeatedly solution deposition process

The mass loadings of $NiCo_2S_4$ on nickel foams could be well-controlled by repeatedly SD process (Sch.1a). As the deposition number increased, the $NiCo_2S_4$ nanosheets gradually covered on the skeleton of nickel foams (Fig.1a-d). The self-

assembled clusters stepwisely become more compact and filled the pore of nickel foams, leading the increasement of mass loading. Moreover, there are no significant change in the cluster structure of $NiCo_2S_4$ mesoporous nanosheets in the repeatedly SD process (Fig.1c-d). The mass loadings uniformly increased during each SD process, exhibiting its high controllability (Fig.2). Low mass volatility in the process means the experimental results can be easily repeated which is very important for scale-up.

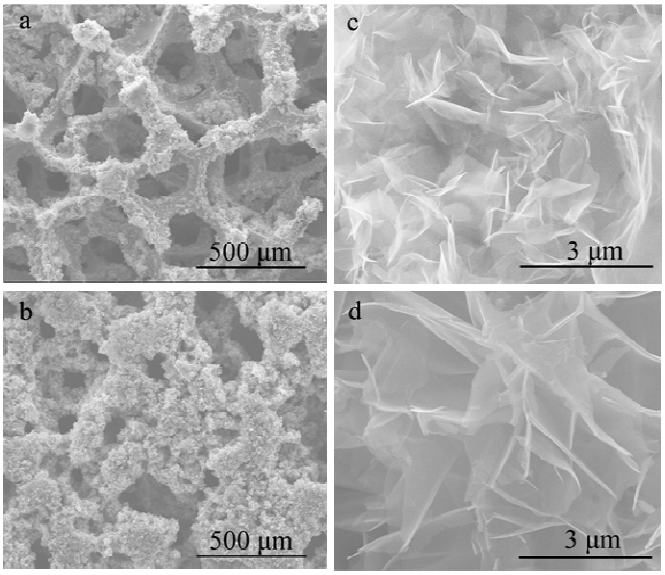

Fig.1 SEM image of $NiCo_2S_4$ with different deposition number on nickel foam.(a)(c), (b)(d) belong to D1, D4, respectively.

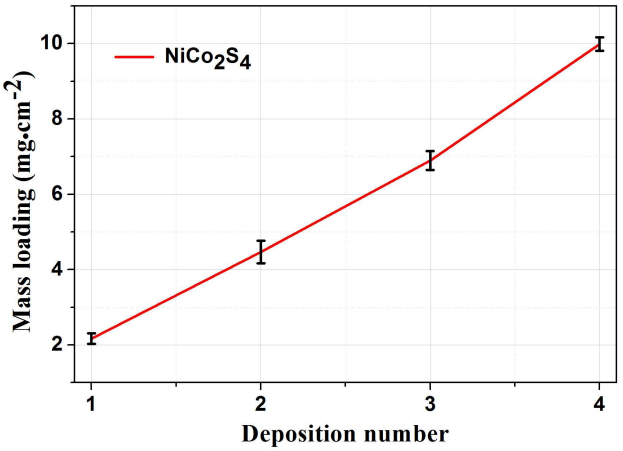

Fig.2 Mass loading of $NiCo_2S_4$ on nickel foams.

Through self-assembly and oriented attachment processes, the self-organization of $NiCo_2S_4$ nanoparticles spontaneous took place, forming 3D interconnected nanosheet clusters on nickel foams.[22,23]The controlled self-assembly process of nanoparticles can lead to the formation of microstructure which provides shortened pathways and facilitates an effective electrolyte penetration, consequently leading to improved capacitance and rate capability.[18]

3.2 Synthesis of $NiCo_2S_4$ mesoporous nanosheets

The $NiCo_2O_4$ precursors are compose of 3D interconnected flower-like nanosheet structure through a SD and annealing process (Fig.3a). After AER, the as-prepared $NiCo_2O_4$ precursors can be easily converted to the corresponding $NiCo_2S_4$ with well-retained 3D interconnected nanosheet morphology (Fig.3c). Obviously, the nickel foams are covered with self-assembled clusters which formed by closely adjacent $NiCo_2S_4$ nanosheet units. XRD patterns confirm the conversion from $NiCo_2O_4$ phase (JCPDF 20-0781) to $NiCo_2S_4$ phase (JCPDF 43-1477) in the AER process (Fig.S1a). EDS patterns of the as-fabricated material also confirm the existence of $NiCo_2S_4$ and the successful conversion of $NiCo_2O_4$ to $NiCo_2S_4$ (Fig.S1b). The element ratio of Ni, Co, S is 1: 2.02:4.05, matching well with the formula of $NiCo_2S_4$.

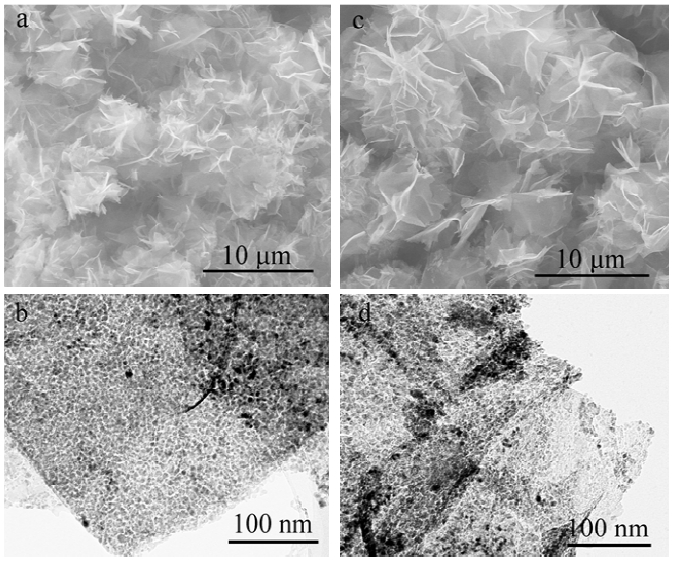

Fig. 3 The transformation from $NiCo_2O_4$ nanosheets to $NiCo_2S_4$ nanosheets. (a-b) SEM and TEM images of $NiCo_2O_4$ nanosheets; (c-d) SEM and TEM images of $NiCo_2S_4$ nanosheets;

To further evaluate the composition of the $NiCo_2S_4$ nanosheets, X-ray photoelectron spectroscopy (XPS) measurements were conducted and the results are shown in Fig.S2. In the Ni 2p XPS spectrum, the deconvolution of the Ni 2p peaks indicates the atoms in $2p_{3/2}$ electronic configuration at 856.5 eV (Fig.S2b), meaning that it was in the divalent and trivalent states.[16] The peak at 874.8 eV corresponds to the Ni $2p_{1/2}$ band. Simultaneously, the Co 2p XPS spectrum shows a doublets which contain a low energy band (Co $2p_{3/2}$) and a high energy band (Co $2p_{1/2}$) at 783.6 and 798.5 eV (Fig.S2c). The spin−orbit splitting value of $Co2p_{1/2}$ and Co $2p_{3/2}$ is over 15 eV, indicating the existence of Co^{2+} and Co^{3+}.[20] As for the S 2p spectrum, the peak at 161.8 eV is characteristics of S^{2-} (Fig.S2d) and the component at 162.9 eV can be ascribed to the sulphion in low

coordination at the surface.[20] According to the above XPS analysis, the $NiCo_2S_4$ sample at near-surface has a composition of Co^{2+}, Co^{3+}, Ni^{2+}, Ni^{3+}, S^{2-}, well matching with the formula $NiCo_2S_4$.

The low-magnification TEM images (Fig.4a-b) confirm the nanosheet structure of the as-prepared $NiCo_2S_4$. When the TEM images (Fig.3d and Fig.4b) magnified, it clearly to observed that the mesopores with the estimated size of 4-7 nm are conformably distributed through the surface of $NiCo_2S_4$ nanosheets. The appearance of lattice fringes as shown in Fig.4d indicates the high conductivity feature of the $NiCo_2S_4$ mesoporous nanosheets.[22,23]The Brunauer-Emmett-Teller (BET) surface area of the obtained $NiCo_2S_4$ is calculated to be as high as 51.74 m^2g^{-1} which tested by the N_2 absorption-desorption measurement at 77 K (Fig.S3a). Moreover, the mesoporous feature of $NiCo_2S_4$ can further proved by the pore-size distribution analysis (Fig.S3b), revealing a pore size arrange of 5-7 nm which is also well consistent with the result of TEM analysis.

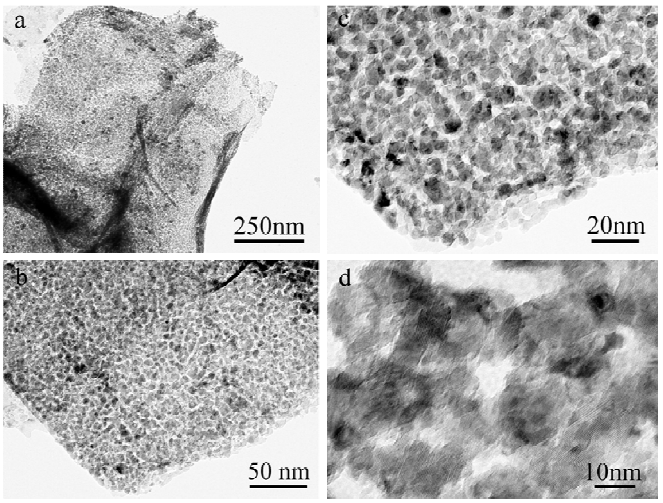

Fig. 4 TEM images of mesoporous $NiCo_2S_4$ nanosheets.

3.3 Electrochemical performance of the as-prepared electrodes

To demonstrate the electrochemical performance of the electrodes with the obtained $NiCo_2S_4$ materials, cyclic voltammetry (CV), galvanostatic charge/discharge measuremen -ts were performed. Obviously, the shapes of the CV curves in Fig.5a are completely different from the ideal rectangular shapes which often show in the CV curves of EDLCs. A pair of redox peaks in the CV curves reveals that the electrochemical performance of the as-prepared electrodes mainly results from their pseudocapacitance (also see the supporting information, Fig.S4a-d) (also see the supporting information, Fig.S4a-d). The integrated CV area for the $NiCo_2S_4$/nickel foam electrode (D1) is obviously larger than the corresponding $NiCo_2O_4$/nickel foam electrode, confirming that the $NiCo_2S_4$ material is more suitable to applying in pseudocapacitors.[16] Moreover, the elect-

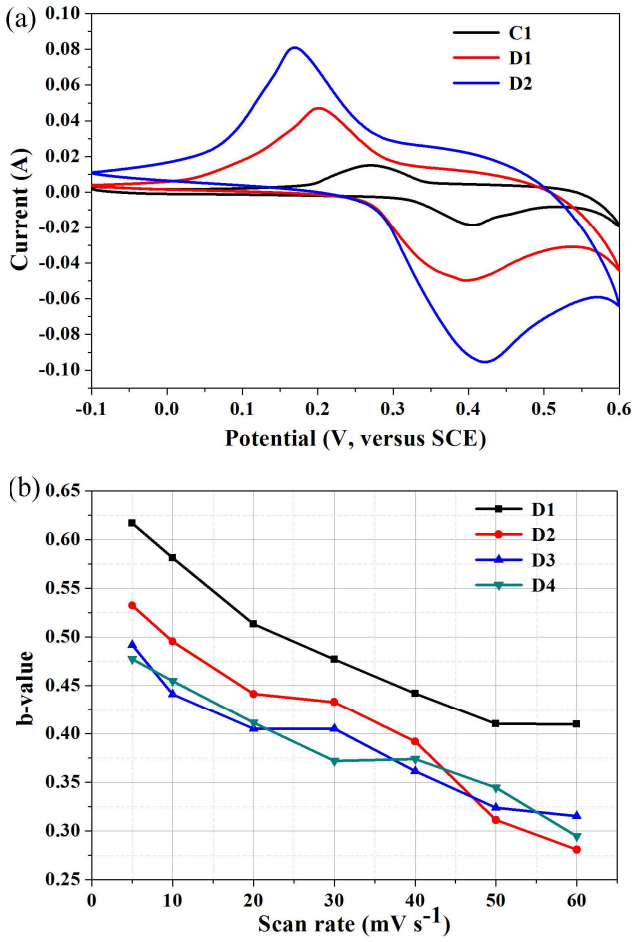

Fig.5 (a) CV spectra of C1, D1, D2 at 5 mVs^{-1}; (b) b values of D1, D2, D3, D4 at scan rates between 5 and 60 mVs^{-1}

rode with high mass loading (D2) shows higher capacitance than the electrode with low mass loading (D1) at the cost of their reversibility which can observed from peak separation. It may cause by the OH^- diffusion in the electrodes that the electrode with low mass loading is faster than the higher one in the rate of OH^- diffusion. The peak current (I) in CV curves obeys a power-low relationship with the scan rate (v) leads to equation (5):

$$I = av^b \qquad (5)$$

Here, a and b are adjustable parameters. It is possible to discern diffusion-controlled process (b=0.5) from surface-controlled process (b=1) when the b value was known (Fig.5b; see also the supporting information, Fig.S4e). For D1, b value range from 0.64 to 0.52 at the scan rates between 5 and 20 mVs^{-1}, indicating that the capacitive contribution from electric double layer; whereas the b value decreased with the increase of scan rate (20 mVs^{-1}), showing that charge storage was dominated by ohmic contributions and diffusion limitations.

The electrodes were also tested by the galvanostatic charge / discharge measurements. The galvanostatic charge/discharge curves are highly symmetrical at low current densities,

revealing an excellent electrochemical reversibility (Fig.6a, see also the supporting information, Fig.S5a-d). Two visible separated plateaus in the charge/discharge process resulting from redox reactions indicate the pseudocapacitive behavior which consistent with the above CV results. At the current dens ity of 10 $mAcm^{-2}$, the specific capacitances (C_m) is about 324, 1575, 1467, 1104, 1083 Fg^{-1} for C1, D1, D2, D3, D4, respectively (Fig.6c). The corresponding areal capacitances (C_s) which is more important in practical applications are 0.71, 3.41, 6.55, 7.61, 10.82 Fcm^{-2} (Fig.6b). With the increment of mass-

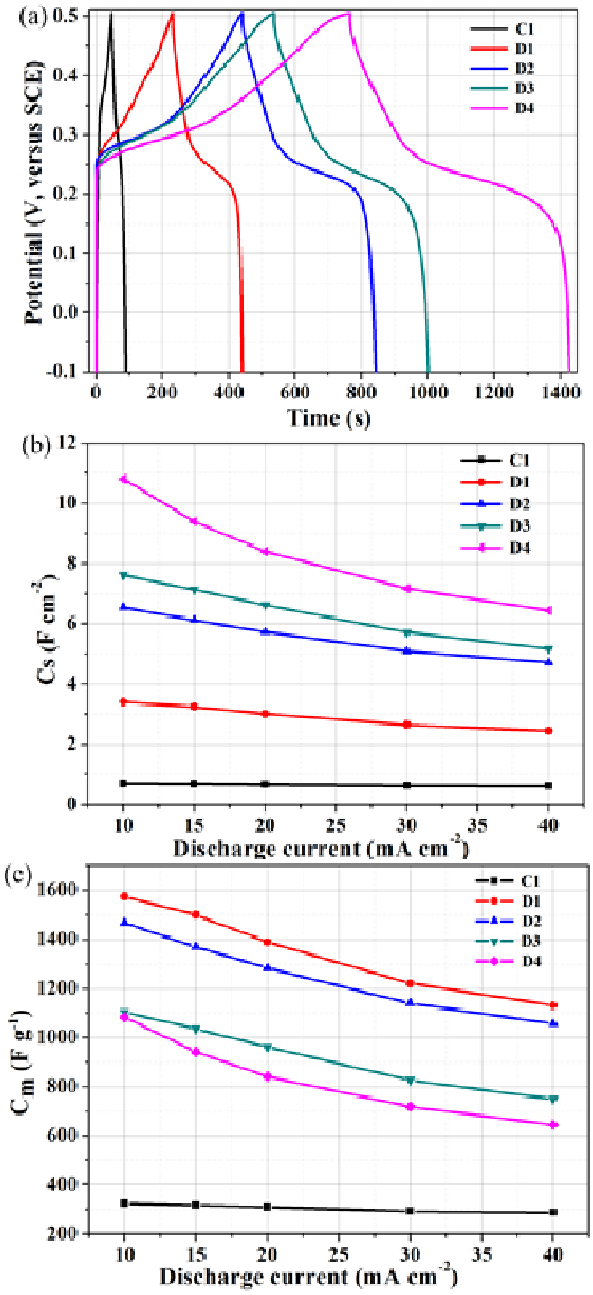

Fig. 6 (a) Charge and discharge curves for C1, D1, D2, D3, D4 at current density of 10 $mAcm^{-2}$; (b) area capacitance (C_s) for C1, D1, D2, D3, D4; (c) specific capacitance (C_m) for C1, D1, D2, D3, D4.

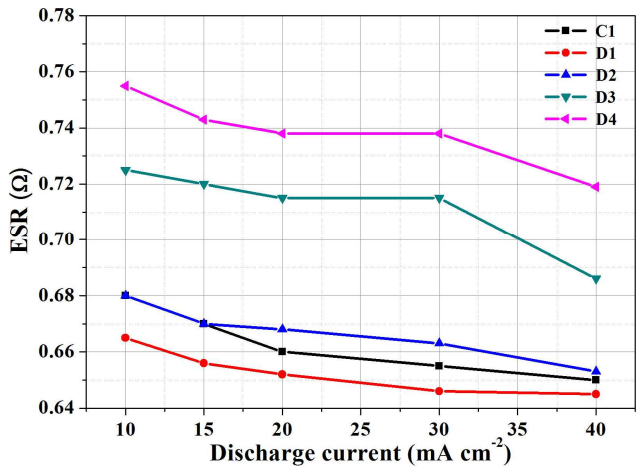

Fig.8 ESR versus discharge density for C1, D1, D2, D3, D4..

loading, the areal capacitances of the $NiCo_2S_4$/nickel foam electrode will increase. On one hand, consistent with the above CV results, the $NiCo_2S_4$/nickel foam electrode (D1) shows significantly higher specific capacitance than the counter $NiCo_2S_4$/nickel foam electrode (C1), even though the amount of active material is slightly smaller. On the other hand, although increased mass loading causes a decreased C_m, the areal capacitances show a contrary trend and more competitive when compared to previous works (see the supporting information, Tab.S1). The electrode of D4 indicates a remarkable areal capacitance of 4.36 Fcm^{-2} even when the current density up to 80 $mAcm^{-2}$. At the result, 40.3% of the capacitance is retained when the current density increased 8-times from 10 to 80 $mAcm^{-2}$, showing the high rate capability of the $NiCo_2S_4$/nickel foam electrode. The decrement of specific capacitance with the increased rate mainly caused by the low diffusion of the electrolyte ions.[7] However, the $NiCo_2S_4$ mesoporous nanosheet structure highly facilitates the ion transfer by providing a short path.[13] Moreover, the high conductivity of the $NiCo_2S_4$ may effectively improve the utilization of the electroactive pseudocapacitive materials even at high rates.[17,20] The interface resistance calculated from electrochemical impedance spectroscopy (EIS) data (Fig.S6) and the equivalent series resistance (ESR) evaluated by means of charge/discharge measurements (Fig.8) can serve as evidence of the high conductivity of $NiCo_2S_4$. The $NiCo_2S_4$/nickel foam electrode (D1) exhibits the ESR value of 0.665 Ω at 10 $mAcm^{-2}$ whereas the corresponding $NiCo_2O_4$/nickel foam electrode (C1) shows the ESR value of 0.681Ω at 10 $mAcm^{-2}$, indicating the higher conductivity of $NiCo_2S_4$ which is consistent with the EIS data (Fig.S6a). The values of ESR for D1, D2, D3, D4 are relatively small and range from 0.648 to 0.752 Ω which is also consistent with the EIS data (Fig.S6b). At the same current density of 10 $mAcm^{-2}$, the values of ESR only increase 13.7% with the mass loading of electrodes increased 4.61-times from 2.168 to 9.984 $mgcm^{-2}$, confirming that the $NiCo_2S_4$ material posses excellent conductivity.

Cycle stability is another key parameter for the electrochemical performance of supercapacitor and D4 was

investigated at current density of 20 $mAcm^{-2}$ with the potential window of -0.1 to 0.51 V for 1500 cycles, as shown in Fig. 9. In the initial cycles, the $NiCo_2S_4$/ nickel foam electrode slightly gained the specific capacitance due to activation of the $NiCo_2S_4$ material.[17] After that, the specific capacitance gradually decreased with the increase of the cycle number, and 92% of the initial specific capacitance retained after 1500 cycles. After 1200 cycles, the specific capacitance nearly keeps stable in subsequent charge/discharge processes. The electrode exhibits a relative long cycle life. During the cycling process, the columbic efficiency remains as high as 90%. According to previous work[18, 24] the cycling performance of the $NiCo_2S_4$ electrode is not outstanding compared to the $NiCo_2O_4$ electrodes and efforts should be paid to address this problem. The relatively good electrochemical stability reveals that a highly reversible redox reaction took place at or near the surface of the electrode without obvious phase change and structural damage of the active material. The 3D interconnected nanosheet morphology of the as-prepared active material is well -retained after 1500 cycles at 20 $mAcm^{-2}$ (Fig.10) which just confirms the above analysis.

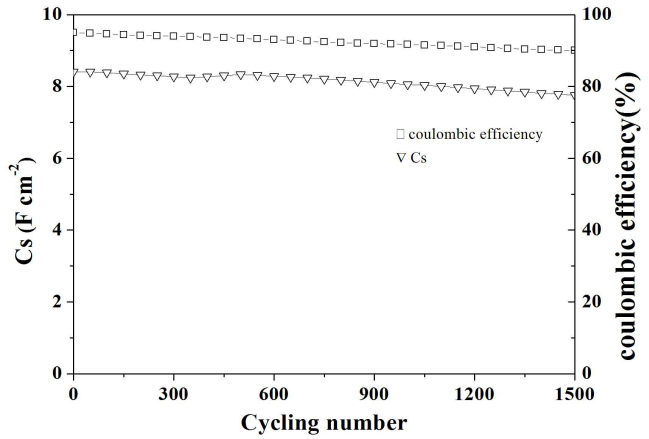

Fig.9 Cycling performance of the $NiCo_2S_4$/ nickel foam electrode (D4) for 1500 cycles at 20 $mAcm^{-2}$.

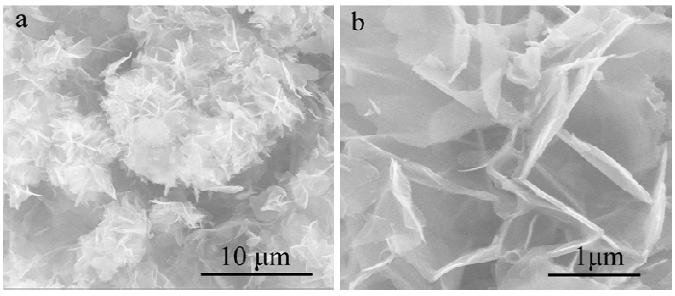

Fig.10 SEM images of the $NiCo_2S_4$ nanosheets on nickel foam after 1500 cycles at 20 $mAcm^{-2}$.

The excellent electrochemical performances of $NiCo_2S_4$ mesoporous nanosheets can be attributed to the following factors. Firstly, the 3D interconnected flower-like nanosheet structure of $NiCo_2S_4$ favors ions efficiently contact with electroactive sites for fast faradic reactions.[10] Secondly, the mesoporous structure of $NiCo_2S_4$ nanosheets provides the efficient path of ion transfer, enhancing the capacitive performance of the electrodes.[13] Thirdly, the high surface area of $NiCo_2S_4$ nanosheets posses many electroactive sites which can significantly facilitates redox reactions at or near the surface of electrodes.[14] Finally, the direct growth of $NiCo_2S_4$ mesoporous nanosheets on nickel foams could ensure good eletron conductivity with the substrate that serves as the current collector.[18]

Conclusions

In summary, the electrodes of $NiCo_2S_4$ mesoporous nanosheets with controllable mass loadings were successfully prepared by a facile two-step solution based method. Owing to the mesoporous nanostructures of $NiCo_2S_4$ and high mass loading, the as-prepared electrodes indicate an excellent electrochemical performance. The as-prepared electrodes exhibits a high areal capacitance (10.82 Fcm^{-2} at 10 $mAcm^{-2}$) , relative good rate performance (40.3% capacitance retention at 80 $mAcm^{-2}$), good cycling stability (92% capacitance retention after 1500 cycles at 20 $mAcm^{-2}$) The excellent electrochemical performance ensure the $NiCo_2S_4$ mesoporous nanosheets as a promising electrode active materials for practical applications. Moreover, it promotes a facile interface design method for control mass loadings of the electrode which might useful in the fabrication of high-performance supercapacitors.

Acknowledgements

This work was supported by National Natural Science Foundation of China (21353003), Special Innovation Talents of Harbin Science and Technology (2013RFQXJ145), Fundamental Research Funds of the Central University (HEUCFZ), Key Program of the Natural Science Foundation of Heilongjiang Province (ZD201219), Program of International S&T Cooperation special project (2013DFA50480).

Notes

Supporting Information

Electronic Supplementary Information (ESI) available: details of any supplementary information available should be included here.

Author Information

a Key Laboratory of Superlight Material and Surface Technology, Ministry of Education, Harbin Engineering University, 150001, PR China.

b State Key Laboratory of Polymer Physics and Chemistry, Changchun Institute of Applied Chemistry, Chinese Academy of Sciences, 130022, PR China.

* Corresponding author: Tel.: +86 451 8253 3026;
fax: +86 451 8253 3026;
E-mail: junwang@hrbeu.edu.cn.

References

1 V. Augustyn, P. Simon and B. Dunn, Energy Environ. Sci., 2014, **7**, 1597.
2 B. E. Conway, V. Birss and J. Wojtowicz, J. Power Sources, 1997, **66**, 1
3 P. Simon, Y. Gogotsi and B. Dunn, Science, 2014, **343**, 1210.
4 A. S. Arico, P. Bruce, B. Scrosati, J. M. Tarascon and W. Van Schalkwijk, Nat. Mater., 2005, **4**, 366.
5 Y. Gogotsi and P. Simon, Science, 2011, **334**, 917.
6 J. Jiang, Y. Li, J. Liu and X. Huang, Nanoscale, 2011, **3**, 45.
7 J. Jiang, Y. Li, J. Liu, X. Huang, C. Yuan, X. W. Lou, Adv. Mater .,2012, **24**, 5166
8 M. Kawamori, T. Asai, Y. Shirai, S. Yagi, M. Oishi, T. Ichitsubo and E. Matsubara, Nano Lett., 2014, **14**, 1932.
9 X. Lang, A. Hirata, T. Fujita and M. Cheni, Nat. Nanotech., 2011, **6**,232.
10 J. Liu, J. Jiang, C. Cheng, H. Li, J. Zhang, H. Gong and H. J. Fan, Adv. Mater., 2011, **23**, 2076.
11 I. E. Rauda, V. Augustyn, B. Dunn and S. H. Tolbert, Acc.Chem. Res., 2013, **46**, 1113.
12 J. N. Tiwari, R. N. Tiwari and K. S. Kim, Pro. Mater. Sci., 2012, **57**, 724.
13 D. Wang, R. Kou, D. Choi, Z. Yang, Z. Nie, J. Li, L. V. Saraf, D. Hu, J. Zhang, G. L. Graff, J. Liu, M. A. Pope and I. A. Aksay, Acs Nano, 2010, **4**, 1587.
14 L. Wang, D. Wang, Z. Dong, F. Zhang and J. Jin, Nano Lett., 2013, **13**, 1711.
15. J. Yang, W. Guo, D. Li, Q. Qin, J. Zhang, C. Wei, H. Fan, L. Wu and W. Zheng, *Electrochimica Acta*, 2014, **144**, 16-21
16 J. Xiao, L. Wan, S. Yang, F. Xiao and S. Wang, Nano Lett., 2014, **14**, 831.
17 P. Yang and J.-M. Tarascon, Nat. Mater., 2012, **11**, 560.
18 G. Q. Zhang and X. W. Lou, Adv. Mater., 2013, **25**, 976.
19 J. Zhang and X. S. Zhao, ChemSusChem, 2012, **5**, 818.
20 H. Chen, J. Jiang, L. Zhang, H. Wan, T. Qi and D. Xia, Nanoscale, 2013, **5**, 8879.
21 H. Wan, J. Jiang, J. Yu, K. Xu, L. Miao, L. Zhang, H. Chen and Y. Ruan, CrystEngComm, 2013, **15**, 7649.
22 H. Colfen and M. Antonietti, Angew. Chem., 2005, **44**, 5576.
23 M. Niederberger and H. Colfen, *Phys.Chem. Chem. Phys.*, 2006, **8**, 3271.
24 X. Y. Liu, Y. Q. Zhang, X. H. Xia, S. J. Shi, Y. Lu, X. L. Wang, C. D. Gu and J. P. Tu, *J. Power Sources*, 2013, **239**, 157.

Graphic Abstract

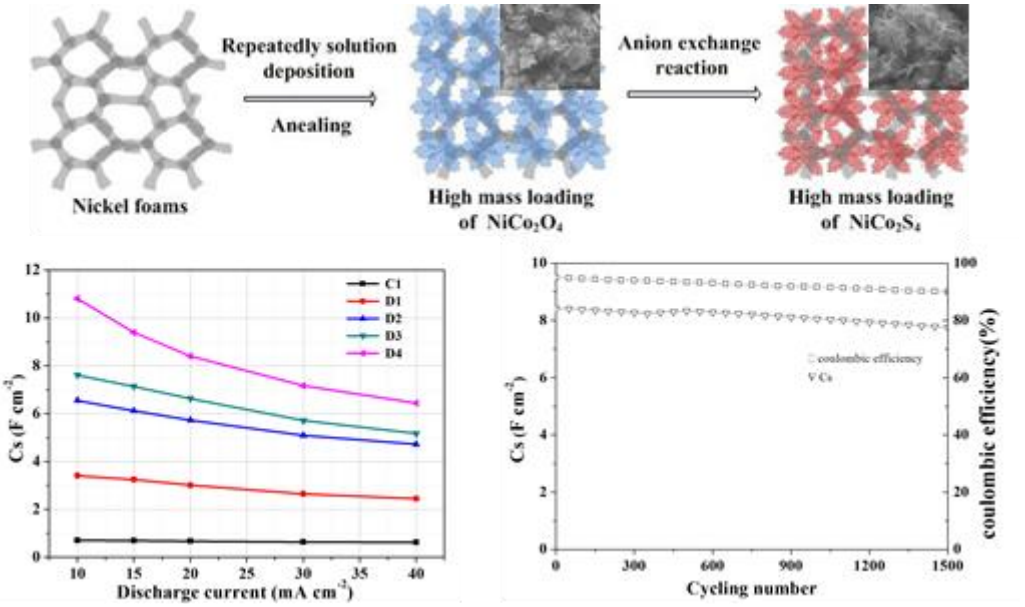

A key challenge for the electrode fabrication is to build up an optimal physical space stepwisely with a large mass loading and guarantees a fast ion and electron transfer.To produce electrodes with controllable mass loadings and microsturctures, High mass loadings could be achieved with increased depositing numbers. Second, considering that high mass loadings always mean the poor ion and electron transportings, and $NiCo_2S_4$ which shows much higher conductivity than $NiCo_2O_4$. Therefore, shape-preserved $NiCo_2S_4$ could be obtained from $NiCo_2O_4$ via a facile anion exchange reaction (AER). As a result, the unique electrode shows excellent performance which make it a promising electrode for supercapacitors. What's more, it may promotes a new interface design method for controlling mass loadings of electrodes for energy storage devices.